Colloid Polym Sci 279:990–1004 (2001)

ORIGINAL CONTRIBUTION

M. L. Rojas-Cervantes
B. Casal
P. Aranda
M. Savirón
J. C. Galván
E. Ruiz-Hitzky

Hybrid materials based on vanadium pentoxide intercalation complexes

Received: 23 January 2001
Accepted: 5 April 2001

M. L. Rojas-Cervantes[1] · B. Casal
P. Aranda · M. Savirón[2] · J. C. Galván
E. Ruiz-Hitzky (✉)
Instituto de Ciencia de Materiales
de Madrid, CSIC, 28049 Madrid, Spain

Present address:
[1]Departamento de Química
Inorgánica y Química Técnica
UNED, c/Senda del Rey s/n
28040 Madrid, Spain

Present address:
[2]Departamento de Química Orgánica
Universidad de Zaragoza
50009 Zaragoza, Spain

Abstract Neutral macrocyclic compounds (crown ethers and cryptands) and charged molecular species (alkylammonium iodides) were intercalated into vanadium oxide xerogel ($V_2O_5 \cdot nH_2O$) to study their influence on the electrical behaviour of this inorganic 2D host lattice. Treatment with alkyl or arylammonium iodide solutions produced the intercalation of organic cations accompanied by the reduction of a fraction of V (V) to V (IV). Characterisation by different techniques allowed the postulation of the interlayer arrangement of the guest species. The study of electrical behaviour at different temperatures indicated that the properties of the hybrid materials can be mainly related to the nature of guest species, the degree of host lattice reduction, the interlayer water content, and the presence of metal ions deliberately introduced in the system.

Key words Vanadium pentoxide xerogel · Macrocycles · Alkylammonium · Electrical conductivity · Nanocomposites

Introduction

According to Livage [1] vanadium (V) pentoxide gels can be described either as hydrous vanadium oxides ($V_2O_5 \cdot nH_2O$) or as poly(vanadic acid) $H_{0.4}V_2O_7 \cdot nH_2O$; its aqueous colloidal dispersions are presented in the form of well-ordered platelets (“tactoids”). The corresponding air-dried solids, i.e., the xerogels ($V_2O_5 \cdot n$-H_2O; $1.4 < n < 1.8$), also show a layered organisation [2], resulting from the stacking of V_2O_5 sheets which are separated from one another by water molecules (Fig. 1).

As the V_2O_5 xerogels (VGs) intercalate a wide variety of compounds [1, 3–7] including conducting polymers [8–13], there is an increasing interest in the use of such hybrid derivatives as electroactive materials for application in different electrochemical devices [12–15]. VGs are n-type semiconductors [16] that can be involved in redox processes with the guest species, with formation of V^{5+}/V^{4+} couples. They are of interest owing to their potential role in the design of materials with electronic conductivity. The nature of the interaction between the inorganic host matrix and the organic guest moiety is crucial for the structural and electronic behaviour. Thus, intercalated ionic or neutral organic species can modify some characteristics of the pristine $V_2O_5 \cdot nH_2O$. The intercalation takes place following different mechanisms, such as charge transfer [6], proton transfer [3, 4], redox [17–19], complexing of interlayer protons [11], and ion-exchange [5]. In some cases, the intercalation mechanism could simultaneously involve several such processes, for instance, those that take place during cationic-dye intercalation [20].

More complicated mechanisms are usually involved in the preparation of conducting polymer/V_2O_5 nanocomposites. In this way, aniline produces an intercalative polymerisation giving polyaniline/V_2O_5 nano-composites following protonation, ion exchange, redox and charge-transfer mechanisms [8, 21, 22]. These nanocomposites exhibit electrical conductivity values ($\sigma = 0.5$–10^{-2} S/cm), which are much higher than those found in

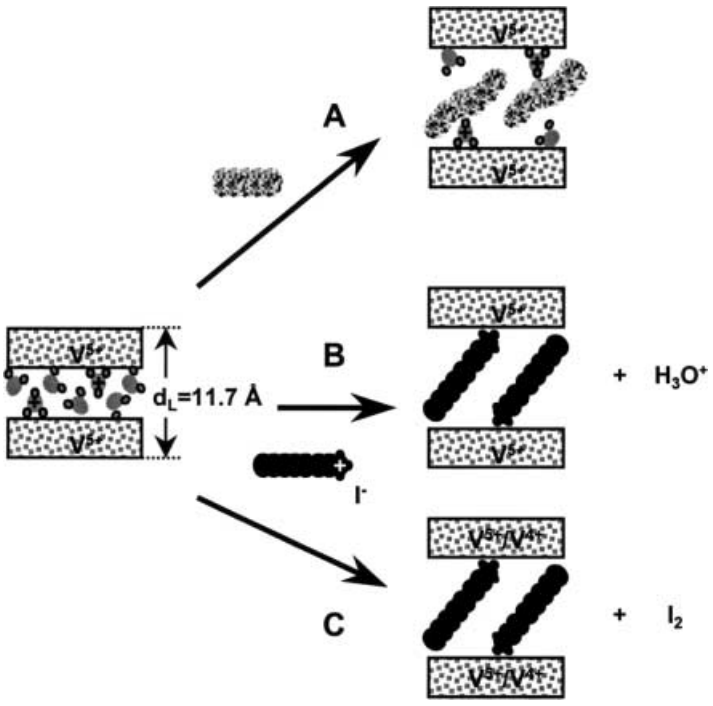

Fig. 1 Schematic representation of mechanisms operating in the intercalation processes of organic species into V_2O_5 xerogel (*VG*): **A** complexation of interlayer cations, **B** ion-exchange, and **C** intercalative redox reactions

composites based on aniline polymerisation into electronically insulator 2D and 3D host lattices (clay minerals, phosphates, arsenates, zeolites, pillared clays, etc.) [23]. Ion-conducting polymers such as poly(ethylene oxide) can be intercalated directly into VG, following a mechanism involving complexation between the oxyethylene units and ionic species present in the interlayer region [10, 11, 24, 25].

In addition to the electrical behaviour related to the n-semiconducting character of V_2O_5, the electrical properties of $V_2O_5 \cdot nH_2O$ strongly depend on the water content. The protons in the interlayer space with mobility lead to relatively high conductivity values [1, 26–30]. The ion conductivity changes dramatically when ammonia or organic bases (pyridine, pyrazine) are intercalated because the protons are captured by intracrystalline acid–base reactions [3, 4].

In view of the preceding results, the objective of this article is to report the electrical behaviour of VGs after intercalation of organic species of two groups: macrocyclic compounds such as crown ethers and cryptand-2,2,2 (C222) as well as alkyl and arylammonium iodides (Fig. 2). The choice of such families of compounds is based on the fact that they modify the electrical properties of $V_2O_5 \cdot nH_2O$ by operating as complexing agents of the interlayer protons with partial replacement of water molecules [11] (Fig. 1A), acting in ion-exchange processes [30] (Fig. 1B), or decreasing the oxidation state of V^{5+} [21, 31] (Fig. 1C). In addition to these three alternative routes we used *N*,*N*,*N*-trimetylammonium-methyl tetrathiofulvalene iodide (TTFRI). It is expected

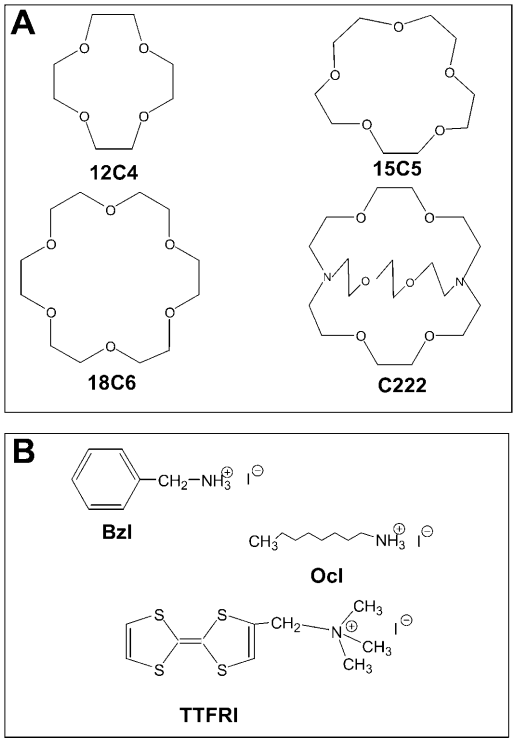

Fig. 2 Guest molecules for intercalation into V_2O_5: **A** 12-crown-4 (*12C4*), 15-crown-5 (*15C5*), 18-crown-6 (*18C6*), and cryptand-2,2,2 (*C222*); **B** benzylammonium iodide (*BzI*), octylammonium iodide (*OcI*), and *N*,*N*,*N*-trimetylammoniummethyl tetrathiofulvalene iodide (*TTFRI*)

that this derivative is intercalated by both ion-exchange and redox mechanisms. In addition, the resulting hybrid material might also show a charge-transfer process between host and guest [6]. This last possibility could also be of interest in view of modifying the electrical behaviour of the xerogel.

Experimental

V_2O_5 xerogel

The VG was prepared by refluxing 10 g orthorhombic V_2O_5 (Analytical Carlo Erba, RPE) and 50 ml *tert*-butyl alcohol (Bu^tOH) (Merck, p.a.), for 6 h. The excess orthorhombic V_2O_5 was separated by centrifugation (11,000 rpm, 30 min). A least 100 ml water was added to the solution [consisting of Bu^tOH and $VO(Bu^tO)_3$], and Bu^tOH was removed in a vacuum rotary evaporator. The dispersion was aged at room temperature for 2 weeks, and a red–brown colloidal dispersion was obtained [3, 20]. Then, self-supporting $V_2O_5 \cdot 1.5H_2O$ xerogel layers were prepared from this suspension by slowly drying a few millilitres onto a Mylard support. The VG films were ion-exchanged with different metal ions (Li^+, K^+, ...) with aqueous solutions of the corresponding nitrates at room temperature.

Guest species

The macrocyclic compounds 12-crown-4 (12C4), 15-crown-5 (15C5), 18-crown-6 (18C6) and C222 were commercial products (Merck, 95–98% purity). The alkylammonium iodides C_6H_5-CH_2-NH_3I (BzI) and CH_3-$(CH_2)_7$-NH_3I (OcI) were synthesised as follows. Benzylamine (Scharlau) and *n*-octylamine (Schuchardt) were neutralised with HI in aqueous solution (57% w/w). The resulting crystalline products were filtered and washed several times with cold diethyl ether (Panreac, p.a.) and *n*-hexane (Sigma-Aldrich high-performance liquid chromatography grade) to remove the excess amine. The ammonium quaternary salt TTFRI was prepared as reported by Fabré et al. [32] for the preparation of amino-TTF derivatives from Li-TTF. Thus, methyl iodide was added to a solution of *N,N*-dimethylaminomethyl-TTF in methanol/diethyl ether up to precipitation of the TTFRI derivative.

Intercalation

Intercalation of the macrocyclic compounds was carried out in two steps: VG films were firstly treated with 1 ml H_2O:methanol (50% vol) mixture for 5 min to provoke a partial swelling of the solid, and then some drops of either pure or highly concentrated solutions of the corresponding macrocyclic compound were added. After 24 h the films were taken off the solution, washed with methanol, and air-dried at room temperature.

Intercalation of the alkyl and arylammonium compounds were carried out as follows. VG films were placed into Petri dishes containing 10 ml BzI/water or OcI/acetone:water (1:1) solutions and kept at room temperature for various time periods (3–22 h). They were removed and washed with an acetone:water mixture (50% vol). Different quantities of the iodides were used to reach final iodide/V_2O_5 molar ratios $r = 0.2$–1.0.

Intercalation of TTFRI was carried by putting a film (10–30 mg) of VG in 15 ml acetonitrile:water (1:2, in volume) mixture in a Teflon reactor and then adding the selected amount of TTFRI (molar ratio iodide/$V_2O_5 = 0.2$, 0.4, and 1.0) in 10 ml acetonitrile. The system was heated for 18 h at 60 °C and then dried for 3 h at 25 °C in a dynamic vacuum dryer to remove residual solvents.

Characterisation techniques

X-ray diffraction (XRD, Philips PW 1710 instrument with a Cu anode and Ni filter), IR spectroscopy (PerkinElmer 580B double-beam spectrophotometer and Nicolet 20SXC Fourier transform IR spectrophotometer), and elemental microanalysis (PerkinElmer 2400 CHN elemental analyser) were used for chemical and structural characterisation. IR studies of thermally treated derivatives were carried out in a conventional Pyrex glass cell that allowed exposure to a vacuum (10^{-3} torr). The thermogravimetric analyses were carried out using a Seiko SSC/5200 thermobalance coupled to a Balzers GDS 300T thermostat mass spectrometer working under a continuous flow of dry He. A Vacuum Generators ESCA LAB MKII spectrometer with a hemispherical analyser (Mg Kα, $E = 1253.6$ eV or Al Kα, $E = 1486.6$ eV radiation) was used for X-ray photoelectron spectroscopy (XPS) studies.

Electrical properties

The electrical properties were studied by electrochemical impedance spectroscopy using a Solartron 1255 frequency-response analyser coupled to a Princeton Applied Research 273A potentiostat/galvanostat. The applied signal amplitude was 50 mV in the 10^5–10^{-2} Hz frequency range. The electrical conductivity was determined either in samples prepared as films with both sides coated with Ag paint or in samples processed as cylindrical pellets (7-mm diameter) with a coating of Au, placed between two platinum grids acting as electrodes. Changes in the electrical behaviour of the samples with temperature were studied in a special cell allowing controlled heating and maintenance of N_2 flow during the measurements.

Results and discussion

Intercalation of macrocyclic compounds

Attempts to intercalate crown ethers into VG directly from organic solutions, using acetonitrile or methanol as solvents as reported for smectite clay minerals [24, 33], yielded derivatives of low organic content and XRD patterns showing irregular stacking of the layers (interstratification). In the case of 12C4 intercalation from methanol, about 0.1 mol crown ether was intercalated per mole of V_2O_5. The corresponding XRD patterns show the existence of a preponderant phase with a basal spacing (d_L) of about 14 Å, and $d_{(00l)}$ reflections characteristic of the pristine VG. Well-ordered crown ether/V_2O_5 hybrids were obtained when the VG was previously expanded with water:solvent solutions (swelling method) as previously reported [11].

Following this method we intercalated several macrocyclic compounds, such as 12C4, 15C5, and 18C6, and a diaza-bicyclic compound, C222, into the V_2O_5 or *M*–VGs ($M = Li^+$, K^+, Ba^{2+}, Ag^+). For *M*–VGs this procedure reveals satisfactory results only for $M = Li^+$ or K^+. Some properties of the derivatives are summarised in Table 1.

Characterisation of macrocycle/V_2O_5 derivatives

XRD patterns of different macrocyclic derivatives are shown in Fig. 3. As discussed elsewhere [11], the increase in the basal spacing compared to the pristine VG is interpreted in terms of 2:1 or 1:1 intracrystalline complex formation, involving macrocycle–H_3O^+ interactions. For 12C4/VG a 2:1 stoichiometry is postulated, with a basal spacing of 20.4 Å, in agreement with the organic content. A 12C4/V_2O_5 intermediate (d_L = 16.6 Å; 0.28 mol of 12C4 per formula) is obtained at shorter reaction times (less than 12 h, at room temperature). An interlayer distance of 16.6 Å results from the coexistence of water molecules, as corroborated by IR, thermal, and chemical analyses. Also, the macrocycle adopts a distorted arrangement (no coplanar oxyethylene units; Fig. 1A). A similar picture can be admitted for 15C5 and 18C6/VG.

The intercalation of C222 causes an increase of about 8 Å, which is in agreement with the molecular thickness of such a ligand and is similar to the values reported for C222 intercalates in clay minerals [33].

Table 1 Basal spacing and composition of macrocyclic/V_2O_5 xerogel (*VG*) intercalation compounds

Derivative	Moles of organic compound per V_2O_5 formula	Basal spacing (Å)	Composition
12C4/VG	0.44	20.4	$V_2O_5(12C4)_{0.44} \cdot 0.54H_2O$
15C5/VG	0.22	16.9	$V_2O_5(15C5)_{0.22} \cdot 0.65H_2O$
18C6/VG	0.19	17.1	$V_2O_5(18C6)_{0.19} \cdot 0.83H_2O$
C222/VG	0.12	17.4	$V_2O_5(C222)_{0.12} \cdot 0.39H_2O$
12C4/Li–VG	0.35	16.3	$Li_{0.26}V_2O_5(12C4)_{0.35} \cdot 0.15H_2O$
15C5/Li–VG	0.27	17.3	$Li_{0.26}V_2O_5(15C5)_{0.27} \cdot 0.03H_2O$
18C6/K–VG	0.07	16.2[a]	$K_{0.26}V_2O_5(18C6)_{0.07} \cdot 0.39H_2O$

[a] Interstratified material

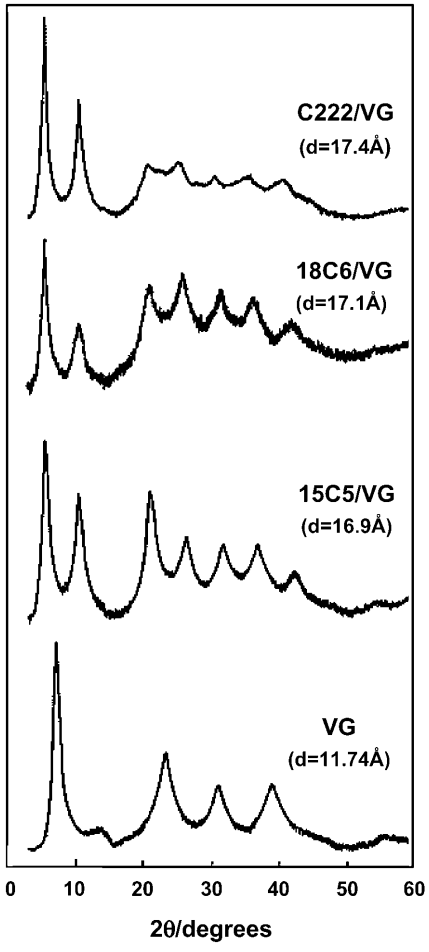

Fig. 3 X-ray diffraction (*XRD*) patterns and basal spacing (d_L) of VG and the 15C5, 18C6, and C222 derivatives

Macrocycle/M–V_2O_5 derivatives

Macrocyclic derivatives obtained from *M*–V_2O_5 ($M = Li^+$ and K^+ ions) matrices always have smaller basal spacings compared to the homologues obtained from the nonexchanged VG. This fact is ascribed to the lower content of water. The intercalation of macrocycles takes place by complexation of the exchangeable alkaline metal ions similarly to the mechanism operating in crown ether/clay mineral complexes [33]. When K–V_2O_5 was used the XRD patterns corresponded to interstratified materials owing to the coexistence of

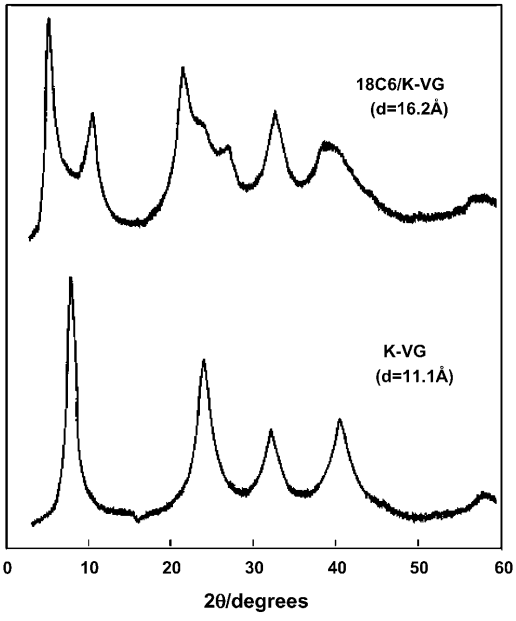

Fig. 4 XRD patterns and d_L of potassium-exchanged VG (*K–VG*) and the 18C6 derivative (*18C6/K–VG*)

intercalated and nonintercalated phases, see, for instance, the XRD diagram of 18C6/K–V_2O_5 (Fig. 4).

Characteristic bands of the guest species [34] together with those of the VG [35] are revealed in the IR spectra of macrocycle/V_2O_5 (Fig. 5). The slight differences in frequencies (Table 2) are ascribed to the host–guest interactions, as in the corresponding clay mineral derivatives [34]. The bands around 1600 cm^{-1} assigned to $\delta_{(H–O–H)}$ vibrations of H_2O in the interlayer space afford information about the nature of the remaining water molecules after intercalation of macrocyclic compounds. It is very important to clarify the role of these molecules in the electrical behaviour of the nanocomposites as discussed later. For instance, this band is shifted from 1620 cm^{-1} in VG to 1635 cm^{-1} in the case of 18C6/V_2O_5, indicating that the remaining water molecules have stronger interactions with the interlayer surroundings. For 12C4 and 15C5/V_2O_5, this band is shifted to 1644 and 1632 cm^{-1}, respectively. A new IR band appears between 1730 and 1710 cm^{-1} for the 12C4 and 15C5 derivatives of the VG and M–V_2O_5 matrices. This band, which is not observable in the spectra corresponding to 18C6 and C222 derivatives, is assigned to $\delta_{(H–O–H)}$ vibrations associated with H_3O^+ species [36]. When protons are exchanged for alkaline metal ions, for example, Li–V_2O_5, the band decreases strongly in intensity and appears as a shoulder, supporting the assignment of this band to H_3O^+ species.

For these intercalations the reaction mechanism is ascribed to interaction of the guest macrocycle molecules with protons (or metal ions in the case of M–V_2O_5) located in the interlayer region, acting as ligands of such ions, as occurs in crown ether complexes formed in homogeneous media [37, 38]. In the case of C222/V_2O_5, the basic character of this macrobicycle compound could partially neutralise the protons of the interlayer

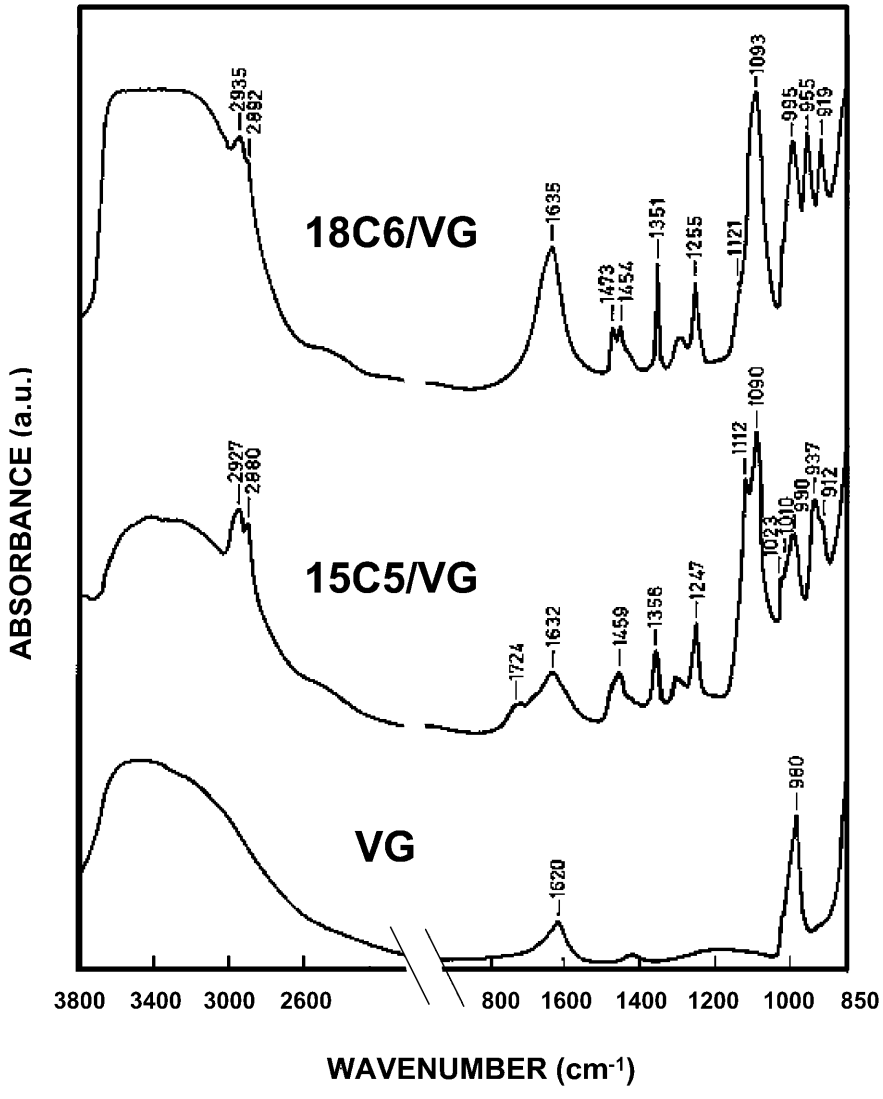

Fig. 5 IR spectra (3800–850 cm^{-1}) of VG and the corresponding 15C5 and 18C6 derivatives

Table 2 Assignation of the IR absorption bands of and intercalation compounds with macrocycles

VG					Li–VG		K–VG	Assignment
	12C4	15C5	18C6	C222	12C4	15C5	18C6	
3,400	3,200	3,400	3,500	3,500	3,500	–	3,512	$\nu_{OH}(H_2O)$
	2,960			2,980	2,977	2,917	2,941	
	2,922	2,922	2,935	2,917	2,922	2,870	2,904	$\nu_{CH}(CH_2)$
	2,874	2,880	2,892	2,884	2,878		2,875	
				2,838				
	1,728	1,724	–	–	1,714	1,724	–	δ_{HOH} (H_3O^+)
1,610	1,644	1,632[a]	1,635	1,620	1,632	1,631	1,616	δ_{HOH} (H_2O)
	1,457	1,473	1,473	1,442	1,482	1,453	1,471	δ_{CH_2} (asym.)
	1,446	1,427	1,454		1,467		1,451	
			1,436		1,445			
	1,365	1,356	1,351	1,380	1,365	1,353	1,350	δ_{CH_2} (w)
				1,354				
	1,304	1,301	1,298		1,301	1,245	1,285	
	1,292	1,290	1,289		1,288		1,250	δ_{CH_2} (t)
		1,247						
	1,133	1,112	1,121	1,128	1,133	1,106	1,107	ν_{CO} (C–O–C)
	1,090	1,090	1,093	1,102	1,093			
1,027[a]	1,025[a]	1,023[a]			1,020[a]			
		1,010		999[a]	1,012	995	993	$\nu_{V=O}$ (V_2O_5)
980	987[a]	990	995[a]	982	986	975	983	
	913	916	920	914	921		915	
		937	955[a]			933	960	δ_{CH_2} (r)

[a] Dichroic bands

space, giving a similar reaction to that observed in the intercalation of other organic bases [4]. This fact explains why the band expected at about 1720 cm^{-1}, assigned to $\delta_{(H-O-H)}$ of H_3O^+ species, was not observed. The bands attributed to $\nu_{(=N-H)^+}$ species in C222 are expected to appear at about 3100–3200 cm^{-1} but they are not observed in the spectra, probably owing to the overlapping of the more intense ν_{O-H} bands associated with the water molecules of the xerogel.

V_2O_5 derivatives prepared by organic–ammonium iodide reactions

Intercalation of organic–ammonium ions into VG takes place in a different way to crown ethers (Fig. 1). Now, two mechanisms are operative: ion-exchange (Fig. 1B) and/or redox (Fig. 1C) processes. Therefore, the VG acts as a cation-exchanger to insert alkyl and arylammonium species from solutions (e.g., water:acetone mixture), replacing protons located in the interlayer region. The maximum number of cations that is expected to be exchanged is of the order of 0.3–0.4 mol per V_2O_5 formula [5, 30]. In addition, it must be that such intercalation induces a partial reduction of the host structure. In this way, it is known that other layered solids containing V (V) species in the structure, such as hydrated vanadyl phosphates and arsenates, react with alkyl and arylammonium iodides giving intercalation compounds that present a fraction of V (V) as V (IV) with charge compensated by the intercalated ammonium cations [39]. Moreover, this method has also been applied successfully to intercalate V_2O_5 with different species [21, 31].

We prepared several V_2O_5 derivatives with different organic–ammonium iodides, such as OcI, BzI, and TTFRI (Fig. 2B). More drastic conditions (swelling and heating) were required to intercalate TTFRI but only a low degree of intercalation was achieved (Table 3).

Benzylammonium–V_2O_5 derivatives

The intercalation of the benzylammonium cation proceeds very quickly. The solution of BzI turned red immediately after introducing the film, owing to the oxidation of I^- to I_3^-. The reaction is almost complete after 3 h, as is deduced from the corresponding intercalation isotherms determined at 3 and 18 h of reaction time (Fig. 6A). For the highest initial BzI/V_2O_5 ratio (1.0), the theoretical and experimental percentage of carbon values are very different (Table 3), indicating that the maximum amount of intercalated benzylammonium is about 0.3 mol BzI per mole of V_2O_5. This value corresponds to the maximum interlamellar coverage that can be reached by ion-exchange, indicating that the arylammonium cations are disposed in a monolayer between the V_2O_5 layers.

Table 3 Composition and structural characteristics of some organic–ammonium/V_2O_5 derivatives

Reagent	Initial iodide/V_2O_5 ratio (r)	Reaction time (h)	%C theoretical[a]	%C experimental	Basal spacing d_L (Å)	Composition
BzI	0.2	3	7.29	6.82	13.5	$V_2O_5(Bz)_{0.17} \cdot 0.61H_2O$
		18		7.47	13.5	$V_2O_5(Bz)_{0.19} \cdot 0.67H_2O$
BzI	0.4	3	13.33	8.61	13.5	$V_2O_5(Bz)_{0.22} \cdot 0.45H_2O$
		18		9.73	13.7	$V_2O_5(Bz)_{0.25} \cdot 0.45H_2O$
BzI	1.0	3	26.50	11.52	13.5	$V_2O_5(Bz)_{0.30} \cdot 0.20H_2O$
		18		11.77	13.8	$V_2O_5(Bz)_{0.31} \cdot 0.35H_2O$
OcI	0.2	6	8.18	4.85	12.4	$V_2O_5(Oc)_{0.11} \cdot 0.89H_2O$
		22		10.28	12.3, 16.8	$V_2O_5(Oc)_{0.24} \cdot 0.38H_2O$
OcI	0.4	6	14.72	10.81	12.4, 16.8	$V_2O_5(Oc)_{0.25} \cdot 0.29H_2O$
		22		13.93	20.5	$V_2O_5(Oc)_{0.33} \cdot 0.29H_2O$
OcI	0.5	6	17.53	16.71	21.0	$V_2O_5(Oc)_{0.41} \cdot 0.34H_2O$
		22		16.82	21.0	$V_2O_5(Oc)_{0.42} \cdot 0.30H_2O$
OcI	1.0	6	28.30	17.71	22.8	$V_2O_5(Oc)_{0.46} \cdot 0.35H_2O$
		22		18.23	24.0	$V_2O_5(Oc)_{0.46} \cdot 0.10H_2O$
TTFRI	0.2	18	9.10	3.03	12.5	$V_2O_5(TTFR)_{0.06} \cdot 1.32H_2O$
TTFRI	0.4	18	15.03	4.73	13.1	$V_2O_5(TTFR)_{0.09} \cdot 1.09H_2O$
TTFRI	1.0	18	24.75	7.74	13.8	$V_2O_5(TTFR)_{0.16} \cdot 1.15H_2O$

[a] Calculated by assuming the general formula: V_2O_5 (organic–ammonium cation)$_r \cdot 1.5H_2O$

Octylammonium–V_2O_5 derivatives

The adsorption isotherms (Fig. 6A) of OcI show that at the lowest initial concentrations of OcI ($r = 0.2$ and 0.4) only half of the intercalated alkyliodide is intercalated after 6 h (Table 3). Kinetic aspects also affect the degree of intercalation. So, complete adsorption is reached after 22 h. However, when higher initial molar ratio are used 6 h of reaction is enough time to reach the maximum intercalation. Thus, for $r = 0.5$ a quantitative intercalation of octylammonium cations is observed although for $r = 1$ only approximately half of the OcI added is effectively intercalated (Fig. 6). Note that the ion-exchange capacity of VG is about 180 mmol per 100 g [5]; for r values greater than 0.5 the host solid has attained its capacity of adsorption. In these cases, the increase in the amount of intercalated octylammonium must be explained by the $V^{5+} \rightarrow V^{4+}$ reduction as is indicated by XPS analyses (Table 4). Nevertheless, the results of the absorption experiments indicate that an ion-exchange process rather than a redox mechanism mainly governs the intercalation process. Similar behaviour is observed for BzI intercalations, although the maximum amount intercalated is lower than for OcI (see later).

TTF derivative intercalation

As indicated earlier, TTFRI intercalation proceeds to a much lower extent than for BzI or OcI, probably owing to the steric hindrance by the large molecule. Thus, the highest amount of TTFR intercalated corresponds to about 0.15 mol TTFR per mole of V_2O_5. These values are smaller than those reported by Van Damme et al. [6] for intercalation of TTF into the VG in ethanol. The presence of this solvent can affect the reduction of vanadium (e.g. $V^{5+} \rightarrow V^{4+}$), which favours the guest insertion. According to those authors [6, 40], their TTF–V_2O_5 organic bronzes are amorphous compounds, in contrast to our V_2O_5 intercalation compounds.

The characteristic XRD diffraction patterns of different organic–ammonium/V_2O_5 derivatives are shown in Fig. 7. When BzI is used, the increase of the basal spacing (4.8 Å) is independent of the benzylammonium content (from $r = 0.2$ to 1.0) and also of the reaction time (3 h). Taking into account the molecular size of benzylammonium ions (around 8.5×4 Å^2) and the value of Δd_L, we conclude that these ions are intercalated in a monolayer with the molecular ring lying almost parallel to the plane defined by the V_2O_5 layers.

In the case of samples intercalated from OcI, the increase in the interlayer spacing depends on the initial iodide/V_2O_5 ratio and the reaction time (Fig. 6B). For low initial ratios ($r < 0.5$) two different phases are obtained by varying the reaction time. Samples prepared from $r = 0.2$ and with 6 h of reaction show a d_L value of 12.4 Å, suggesting the formation of a monolayer of octylammonium ions lying parallel to the V_2O_5 layers; however, samples prepared from the same initial ratio but after 22 h of reaction reveal two values of d_L: 12.3 and 16.8 Å. This fact might indicate the coexistence of two phases, one of them with the alkyl chain of cations lying flat with respect to the V_2O_5 layers and the other with the alkyl chains tilted with respect to the V_2O_5 layers. For samples with $r > 0.5$ a single phase is always obtained with d_L between 21 and 24 Å, corresponding to tilted chains [30].

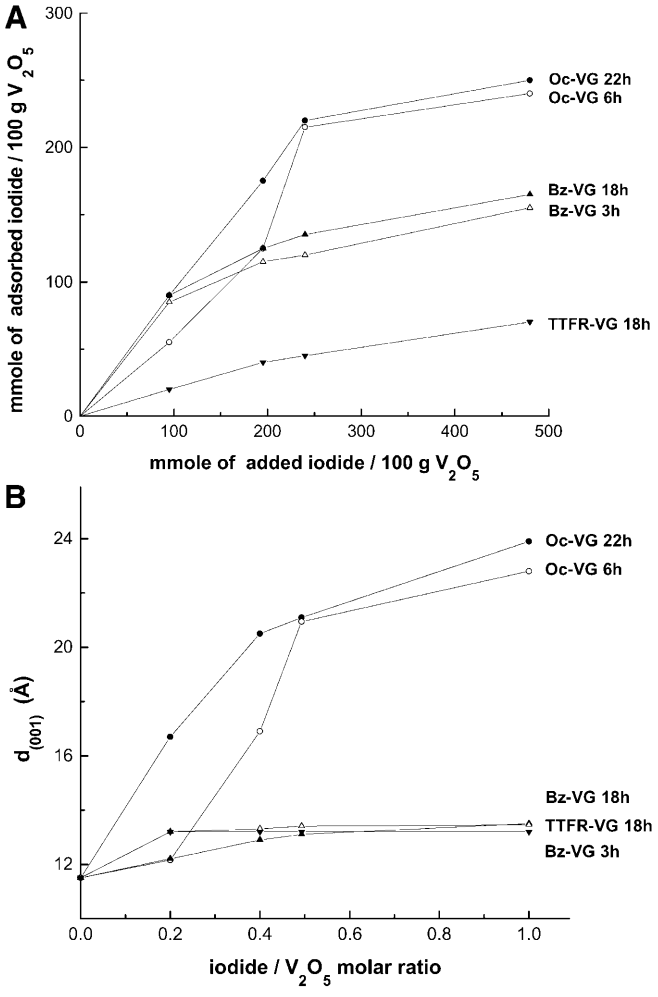

Fig. 6 **A** Intercalation isotherms of TTFRI, BzI, and OcI into $V_2O_5{\cdot}nH_2O$ xerogel after different reaction periods: TTFR–VG (18 h), Bz–VG (3 h), Bz–VG (18 h), Oc–VG (6 h), Oc–VG (22 h); **B** d_L as a function of the initial molar ratio $r = \text{iodide}/V_2O_5$ for some intercalation compounds after different reaction periods: TTFR–VG (18 h), Bz–VG (3 h), Bz–VG (18 h), Oc–VG (6 h), Oc–VG (22 h)

Table 4 Percentage of V (IV) in Oc–VG and Bz–VG deduced from X-ray photoelectron spectroscopy analyses in samples with different organic–ammonium content

Sample	Oc or Bz amount adsorbed (mmol/100 g)	V (IV) (%)	d_L (Å)
Oc–VG	19	8.4	12.3
	64	14.6	12.6
	42	13.9	12.5
	228	22.8	21.0
	154	23.3	20.5
Bz–VG	52	10.7	13.8
	47	8.1	13.8
	90	13.7	13.9
	125	18.1	13.8
	162	8.5	14.0

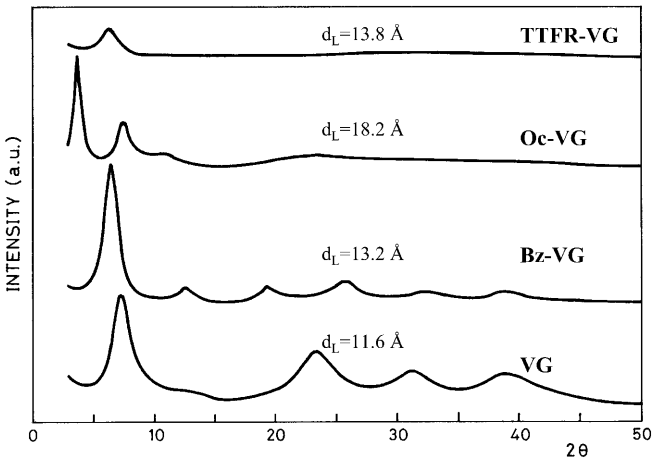

Fig. 7 XRD patterns of $V_2O_5{\cdot}1.5H_2O$ (VG) and some intercalation compounds: Bz–VG ($r = 1$; 18 h), Oc–VG ($r = 1$; 22 h), TTFR–VG ($\mathbf{r} = 1$; 18 h). r = initial iodide/V_2O_5 molar ratio

The TTFR derivatives show Δd_L values of around 4.5 Å, which are practically independent of the amount intercalated. These data suggest that the molecular planes of these organic cations lie parallel to the xerogel layers.

The IR spectra of the xerogel and the derivatives are shown in Fig. 8. The frequencies and assignation of the observed bands are given in Table 5. For the VG the broad band in the 3800–3100 cm^{-1} region, centred at approximately 3400 cm^{-1}, is assigned to the O–H stretching vibration modes of water molecules present in the interlayer space. When BzI is intercalated only two well-defined bands are observed. The octylammonium/V_2O_5 and TTFR/V_2O_5 intercalation compounds generally increase the optical density, producing strong light scattering at 4000–3000 cm^{-1}. In addition to this phenomenon, which was also reported by other authors after intercalation of tetrathialfulvalene into V_2O_5 [6, 41], the absorption due to the C–H stretching vibration of TTF is overlapped by the O–H vibrations bands of the interlayer water.

In the 1800–1500 cm^{-1} region, characteristic bands of the functional groups overlap, which makes their assignation difficult. The band appearing between 1610 and 1622 cm^{-1} can be assigned to the deformation vibrations of either H_2O or NH_3^+ species. In the case of TTFR–V_2O_5 the symmetric N–H deformation mode of the $-NH_3^+$ groups, which is observed at 1504 cm^{-1} in the OcI derivative, is masked by the C=C sharp band of the stretching mode of the ring. In addition, in the 1470–1300 cm^{-1} region, the bands corresponding to δ_{C-H} of CH_2 and CH_3 groups are present in all the intercalation compounds, and the bands appearing in the 1200–1000 cm^{-1} region are assigned to the ν_{C-N} stretching vibrations. The ring stretching vibration bands of TTFR–V_2O_5, which in pure TTFRI arise at

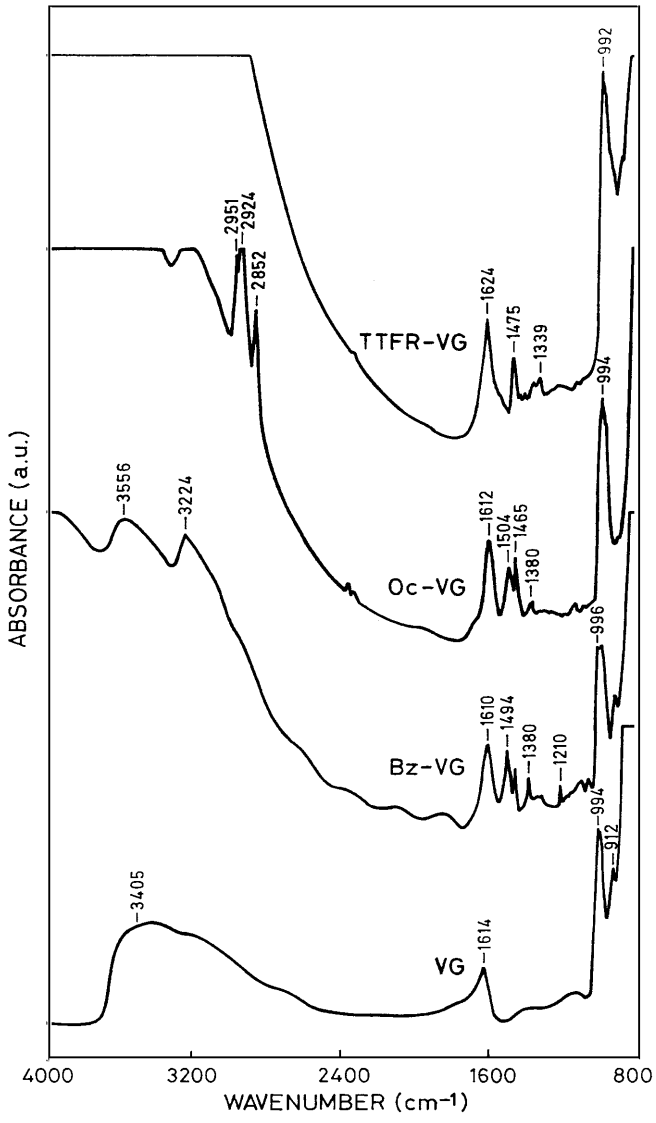

Fig. 8 IR spectra of $V_2O_5{\cdot}1.5H_2O$ (VG) and some intercalation compounds: Bz–VG ($r=1$; 18 h), Oc–VG ($r=1$; 22 h), TTFR–VG ($r=1$; 18 h). $r=$ initial iodide/ V_2O_5 molar ratio

1538 $\nu_{(C=C)}$ and 1252 $\nu_{(C-CH)}$ cm^{-1}, are seriously perturbed since they are replaced by one single vibration at 1339 cm^{-1}. This is in agreement with results observed by Van Damme and coworkers for the intercalation of TTF in V_2O_5 [41] and smectites [42].

Other bands of interest are $\nu_{V=O}$ at 1100–900 cm^{-1}. The IR band located at 1113 cm^{-1} in V_2O_5 is attributed to the elongation mode of the short vanadyl bond [43]. In the original xerogel, two bands are present at 994 and 984 cm^{-1} and the other one at 912 cm^{-1}. The band centred at 912 cm^{-1} is assigned to $\nu_{V=O}$ involved in hydrogen-bonding interactions with the remaining interlamellar water molecules according to Vandenborre et al. [35].

Electrical behaviour

The VG is a mixed ionic–electronic conductor because of the presence of proton species associated with water molecules in the interlayer region and V^{5+}/V^{4+} pairs, which are responsible of the electronic conductivity [1]. In this study we determined the total electrical conductivity (i.e., $\sigma_{ac}=\sigma_i+\sigma_e$) of the intercalation materials by impedance spectroscopy. This technique also appears to be a very useful tool to obtain information about the dynamics of charge carriers and the rotational motion of water molecules bound to the V_2O_5 network [1, 28].

Macrocycle/V_2O_5 derivatives

Typical Nyquist plots for $V_2O_5 \cdot 1.5H_2O$ at different temperatures and also for $15C5/V_2O_5$ selected as a representative example of crown ether intercalation compounds are shown in Fig. 9. For the frequency range used in the present work, the Nyquist plots consist of a single semicircle. The corresponding electrical equivalent circuit may be represented approximately by a parallel combination of a resistor and a capacitor. This capacitive semicircle usually appears depressed, its centre being below the real axis. In such a case, the impedance response of the system, Z^*, is expressed by the Cole–Cole model:

$$Z^* = Z_\infty + (Z_0 - Z_\infty)/[1 + (i\omega\tau)^{1-\alpha}] \ , \quad (1)$$

$$\tau = 1/2\pi f_0 \ , \quad (2)$$

$$\theta = \alpha(\pi/2) \ , \quad (3)$$

where Z_∞ and Z_0 are the impedance at infinite and zero frequency, (i.e., the intersections of the semicircle with the real axis), $\omega=2\pi f$ is the angular frequency, f_0 the resonance (Debye) frequency, τ the time constant, and θ the angle between the real axis and the straight line from the Z_∞ point to the centre of the semicircle. The empirical parameter α is related to the deviation of the impedance plot from the ideal Debye behaviour, $0 \le \alpha < 1$.

We used the values of the two intersection points of the arc with the real axis, i.e., Z_0 and Z_∞, to determine the total electrical resistance of the material, $R_{ac}=Z_0-Z_\infty$. The reciprocal value of this resistance is the alternating current conductivity (σ_{ac}). In this case, it can be ascribed to ionic conductivity (σ_i), because the main conducting carriers are the protons originating from dissociation of adsorbed water at the oxide–water interface [1, 29, 41]. The proton conductivities obtained at room temperature for xerogel films and some crown ethers/V_2O_5 derivatives are given in Table 6. The desorption of water at room temperature produced by flowing dry N_2 decreases the conductivity of the films. In general, the conductivity of VGs strongly depends on the initial state of drying. For this reason Livage [1] noted

Table 5 Assignation of the IR absorption bands of VG and some derivatives: Bz–VG [$V_2O_5(Bz)_{0.31}{\cdot}0.35(H_2O)$; ($r$ = 1, 18 h)], Oc–VG [$V_2O_5(Oc)_{0.46}{\cdot}0.10(H_2O)$; ($r$ = 1, 22 h)], and TTFR–VG [$V_2O_5(TTFR)_{0.16}{\cdot}1.15(H_2O)$; ($r$ = 1, 18 h)]. r = initial iodide/V_2O_5 molar ratio

VG	Bz–VG	Oc–VG	TTFR–VG	Assignation
3,405	3,586			$\nu_{(OH)}$ (H_2O)
	3,224			
		2,951		$\nu_{(CH-)}$ (CH_3) asym.
		2,924		$\nu_{(C-H)}$ (CH_2) asym.
		2,852		$\nu_{(C-H)}$ (CH_2) sym.
1,614	1,610	1,612	1,624	$\delta_{(HO)}$ (H_2O), $\delta_{(NH)}$ (NH_3^+) asym.
		1,504		$\delta_{(NH)}$ (NH_3^+) sym.
	1,494		1,480	$\nu_{(C=C)}$ (ring)
	1,452			
		1,465	1,468	$\delta_{(CH)}$ (CH_3) asym.
	1,380	1,390	1,368	$\delta_{(CH)}$ (CH_3)
	1,312	1,378	1,312	$\delta_{(CH)}$ (CH_2)
	1,344		1,339	$\nu_{(C=C)}$ (ring)
	1,210			–
1,113	1,096	1,149	1,136	$\nu_{(C-N)}$
	1,053	1,100	1,096	
994	998	994	994	$\nu_{(V=O)}$
984	984	982	910	
912	916	913		

serious discrepancies among conductivity values reported in the literature.

The ionic conductivity exhibits anisotropic behaviour. The conductivity is 3 or 4 orders of magnitude larger when the measurements are carried out in a direction parallel to the xerogel layers in comparison to the perpendicular orientation. We did not get information about the electronic component of the conductivity (σ_e) because it required the application of some complementary techniques, such as direct current conductivity measurements [29, 41] or direct current polarisation techniques [44].

The values of the capacitance, obtained from the Nyquist plots of Fig. 9 [45, 46], are of an order of magnitude of 10^{-10} F for V_2O_5 and 10^{-11} F for crown ether/V_2O_5 (Table 6). These values confirm that the semicircles on the Nyquist plots can be ascribed to ionic conduction [47]. In such cases, C represents the geometric capacitance (C_g) of the samples, which is associated in parallel with a resistor, R, corresponding to the ionic resistance (R_i) of the material. C_g depends on the geometric factor of the samples (i.e., their thickness/area relation) and on the dielectric constant, which indirectly depends on the water content of the sample. The strong changes in the capacitance of the V_2O_5 derivatives are ascribed to the replacement of water by the crown ether molecules.

An important parameter deduced from the Nyquist plots is the time constant of the equivalent circuit. The time constant is closely related to both the electrical resistance and to the capacitance by means of the relation $\tau = RC$. It provides information about the relaxation time of carriers in the conduction process, which is also related to the resonance frequency, f_0, by Eq. (2). It shows the time scale of the molecular reorientation.

The dependence of f_0 on temperature also provides information about the dynamic properties of the carrier species [29]. The values of the resonance frequency are deduced from the top of the semicircles on the Nyquist plots. The f_0 values increase gradually upon heating the samples (Fig. 9A). By thermal activation the interaction of the water molecules with their environment becomes so weak that the rotational motion of the water molecules becomes faster and the relaxation time shorter.

At high frequency values (above 10^3 Hz) the impedance response of the VG clearly shows a deviation from a semicircle (Fig. 9A). The interaction of time constants [48, 49] associated with other phenomena that are not observed in our experimental frequency range might be responsible for this deviation. In this way, Badot and et al. [28], using dielectric measurements in the 10^{10}–10^5 Hz frequency range, observed the presence of some additional semicircles associated with different time constants. These time constants were ascribed to dielectric relaxation phenomena arising from the rotation of dipolar species: protonated water molecules (at very high frequencies), water molecules weakly bonded to the oxide network (high frequencies), and strongly bonded water molecules (medium frequencies). In that study the effects due to the electrical (proton) conduction appear at low frequencies, which are close to the high frequencies used in our experiments. Note that the measurements carried out in the present work are in the 10^5–10^{-2} Hz range, allowing the knowledge of the electrical behaviour of VG to be increased from 10^{10} to 10^{-2} Hz.

The conductivity changes of the xerogel with the temperature define two straight lines, from 20 to 110 °C and from 110 to 200 °C, in the Arrhenius plot (Fig. 10). It can be ascribed to the protons generated by the

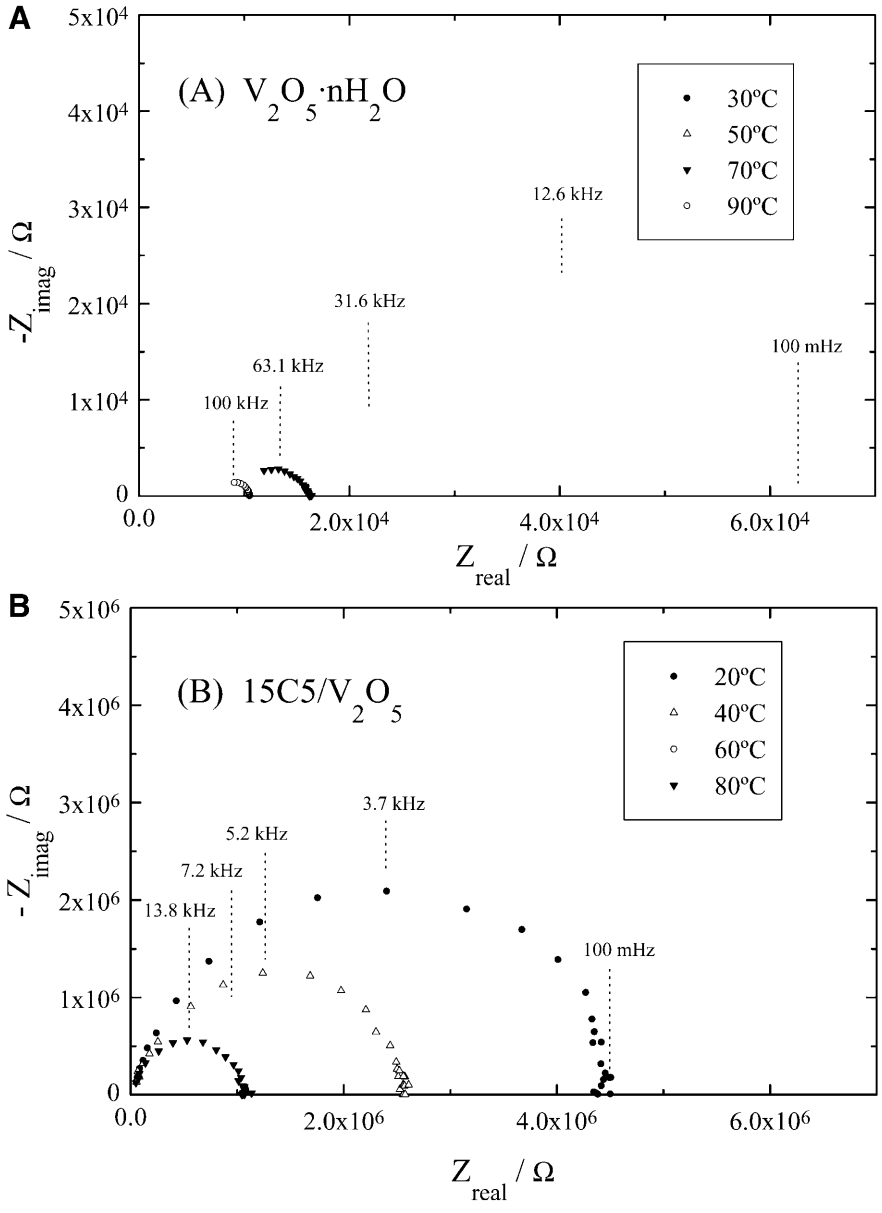

Fig. 9 Impedance spectra (Nyquist plots) measured at different temperatures for **A** $V_2O_5 \cdot 1.5H_2O$ and **B** $15C5/V_2O_5$

dissociation of water in the interlayer space. The corresponding activation energies for the proton conductivity above and below 110 °C are 0.41 and 0.62 eV, respectively. This confirms the presence of two types of water molecules, which is also indicated by the thermal analysis studies of other authors [1]: water molecules weakly bonded to the oxide network that are eliminated up to 120 °C and chemically adsorbed water molecules that remain strongly bonded to the oxide network and which are removed between 110 and 200 °C.

The semicircles in the Nyquist plots for different crown ether/V_2O_5 derivatives have, in general, larger diameters than the parent VG (Fig 9). This behaviour arises from the existence of oxyethylene–H^+ interactions

Table 6 Activation energy, proton conductivity, and geometric capacitance determined by impedance measurements at 30 °C, for VG and related intercalation compounds with macrocyclic ligands

Sample	Activation energy (eV)[a]	Conductivity (Scm^{-1})	Capacitance (pF)
VG	0.3	1.6×10^{-6}	189
12C4/VG	0.3	5.8×10^{-8}	12.2
15C5/VG	0.2	2.9×10^{-8}	12.2
18C6/VG	0.3	2.5×10^{-7}	29.3
C222/VG	0.2	3.2×10^{-8}	16.6

[a] Determined from the Arrhenius plot (20–200 °C)

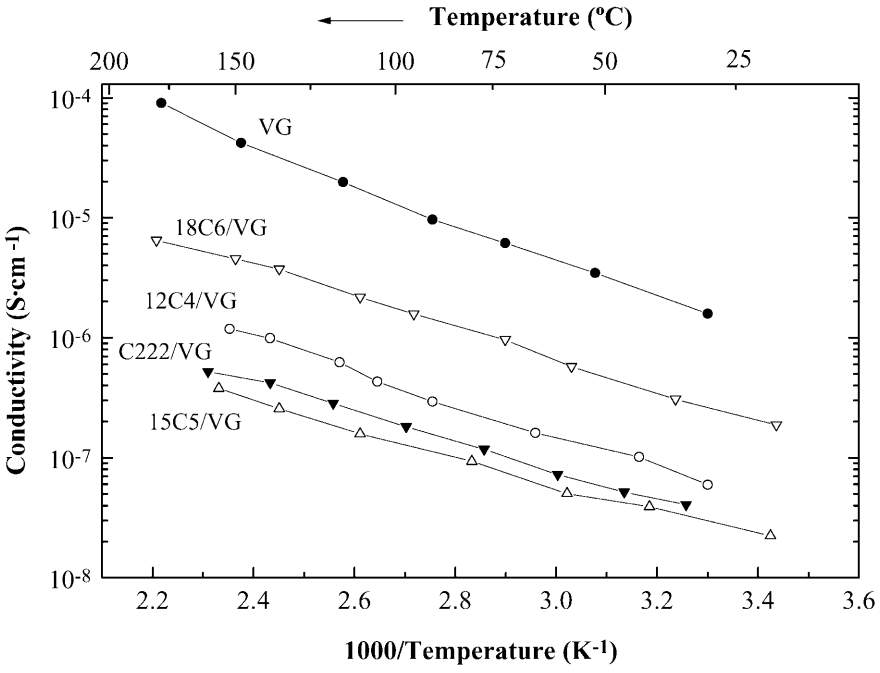

Fig. 10 Conductivity from impedance measurements carried out in the plane parallel to the V_2O_5 layers, at 20–200 °C, for VG and the corresponding 12C4, 15C5, 18C6, and C222 derivatives (12C4/VG, 15C5/VG, 18C6/VG, and C222/VG)

(complexing and disfavouring the mobility of the interlayer protons) and the lower water content after intercalation of the crown ethers. Figure 10 shows that the alternating current conductivity of the V_2O_5 films between 20 and 200 °C is always higher than that of the crown ether/V_2O_5 derivatives.

Table 6 presents the ionic conductivity values at room temperature and the activation energies for 20–200 °C. It is clear that the presence of oxyethylene compounds in the interlayer region decreases the ionic conductivity associated with proton species. This behaviour is opposite to that observed in materials obtained by intercalation of the same oxyethylene compounds into homoionic phyllosilicates [24, 50]. This fact is explained assuming that the proton species in the starting VG are in a quasiliquid medium that allows an almost free mobility of those ions under the applied electric field. Although the presence of oxyethylene compounds increases the separation between the layers, it reduces the ionic mobility owing to their close packing in the interlayer region and to the interaction between the protons and oxygens of the guest molecules.

When the interlayer protons are replaced by alkaline cations, such as K^+, the ionic conductivity decreases (Fig. 11) because these cations are less mobile than protons and the water content is lower.

Summarising the previous results, it can be pointed out that the intercalation of oxyethylene compounds into $V_2O_5 \cdot nH_2O$ xerogels produces strong changes in the electrical properties of the parent host solid and decreases its ionic conductivity. The reason is the reduced mobility of the protons because of complexation of interlayers protons by the oxyethylene compounds and the lower water content after intercalation.

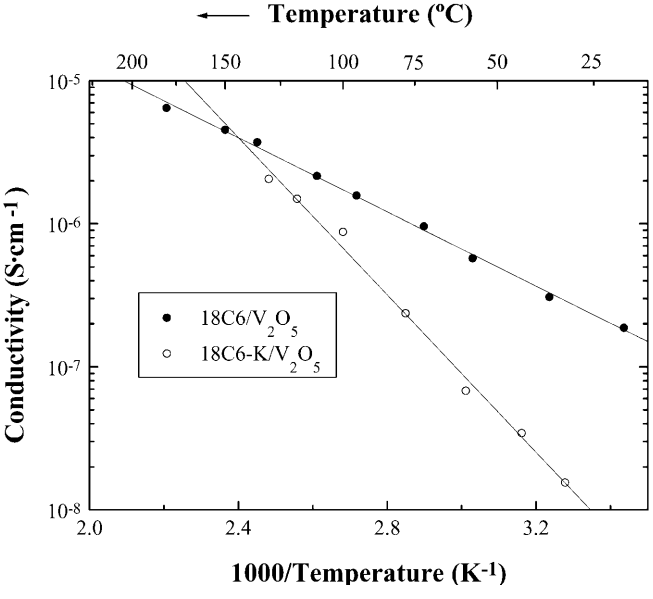

Fig. 11 Conductivity from impedance measurements carried out in the plane parallel to V_2O_5 layers, at 20–200 °C, for 18C6/V_2O_5 (18C6/VG) and 18C6–K/V_2O_5

Organic–ammonium V_2O_5 derivatives

A second part of the electrical study concerns V_2O_5 intercalated by different iodides (OcI, BzI, and TTFRI). The choice of these guest molecules was determined by the fact that they could modify the electrical properties of the VG host lattice in a different manner than the crown ethers. The intercalation of these organic cations proceeds by different mechanisms, such as ion-exchange, redox processes, protonation reactions, or charge-transfer interactions. Moreover, the intercalation involves simultaneously several of these processes. For instance, intercalation of TTFRI is accompanied by the reduction of V (V) to V (IV) and also by a charge transfer between the host lattice and the TTF derivative. Both phenomena increase the electrical conductivity; however, the alternating current conductivity values found for TTFR/V_2O_5, at 20–100 °C, do not present substantial changes with respect to those of the parent xerogel (Fig. 12). The reason is the low degree of intercalation probably owing to the steric hindrance.

The intercalates of the alkyl and arylammonium iodides, where only the reduction of V (V) is operative, show Arrhenius behaviour between 20 and 110 °C (Fig. 12). The corresponding activation energy lies between 0.3 and 0.5 eV. For octylammonium–V_2O_5 the electrical conductivity strongly depends on the geometric arrangement of the organic molecules in the interlayer space and on the degree of intercalation. Thus, for instance, at 60 °C the conductivity decreases, as far as 1 order of magnitude, when the initial OcI/V_2O_5 molar ratio increases from 0.2 to 1.0 (Fig. 12). It should be recalled that for the 0.2 ratio the alkyl chains show a parallel arrangement with respect to the V_2O_5 plane, whereas the chains are in an almost perpendicular arrangement at initial ratios above 0.5. Owing to the increased interlayer distances the conductivity measured in the perpendicular direction is reduced in spite of increased V (V)/V (IV) ion pair formation by the reduction by iodide ions.

The intercalation of benzylammonium ions yields materials with slightly increased conductivity in comparison with the parent $V_2O_5 \cdot 1.5H_2O$ xerogel. The interaction between the aromatic ring and the parallel V_2O_5 layer does not have a significant strength that could enhance the electrical conductivity in the perpendicular direction.

After heating above 110 °C, the conductivity of all these materials (i.e., octylammonium–VG, benzylammonium–VG, and TTFR–VG) does not follow Arrhenius behaviour. From that temperature the conductivity slightly increases and even decreases above 140 °C. This behaviour is a consequence of the progressive degradation of the intercalated organic matter by a pyrolysis processes. Finally, between 190–205 °C, when the organic compound is completely eliminated, the conductivity observed is similar to that found in the VG. The impedance plots then present an accumulation of points on the real axis in the 10^5–1 Hz frequency range, defining a pure electrical resistance, related to the electronic conductivity of the material. The accumulation of data points is followed by a pseudoinductive loop at low frequency, which is typical of unstable systems. In fact, V_2O_5 exhibits pronounced electrochemical reactivity

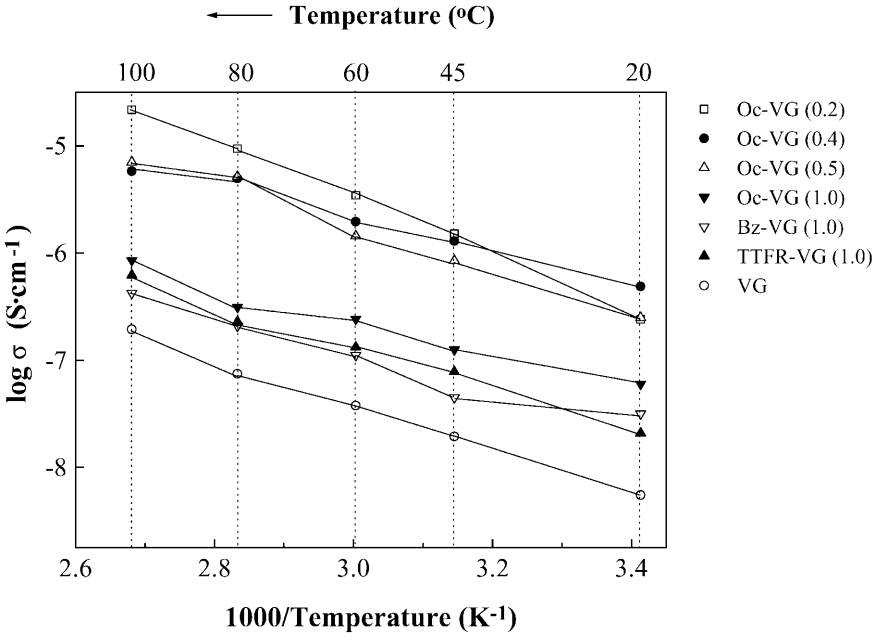

Fig. 12 Conductivity from impedance measurements carried out in the plane perpendicular to the V_2O_5 layers, at 20–100 °C: VG and the intercalation compounds Oc–VG ($r = 0.2$, 0.4, 0.5, and 1), Bz–VG ($r = 1$) and TTFR–VG ($r = 1$). r = initial iodide/ V_2O_5 molar ratio

strongly increasing with the temperature. These results indicate that the organic matter in contact with the xerogel is rapidly oxidised and that the guest molecules are degraded during the impedance measurements.

Concluding remarks

Intercalation of oxyethylene compounds (crown ethers) and organic–ammonium species into VG change significantly the electrical behaviour. The electrical conductivity of these materials depends on many parameters, such as the nature and number of the intercalated guest species, their arrangement between the oxide layers, the degree of reduction of vanadium in the host lattice, and the interlayer water content.

The main conclusion derived from the present results is the low stability of the intercalated organic compounds prepared from iodide salts, which are easily oxidised by V (V) of the host lattice. The great reactivity of V_2O_5 layers leads to impedance diagrams with pseudoinductive loops, which are specially evidenced at low frequency values. The organic–ammonium iodides react with the VG, decreasing the V^{5+}/V^{4+} ratio and, thereby, enhancing the electronic conductivity. This behaviour is promoted by a further reduction of the host lattice owing to the oxidation of the alkyl (and to a minor extent of the aryl) chains.

The intercalation of crown ethers, which replace water molecules in the interlayer space, strongly varies the ionic conductivity associated with proton mobility. Hydronium species are complexed by the oxyethylene ligands. The corresponding impedance measurements show typical diagrams with semicircles that give information on the electrical parameters of those compounds. These crown ether/V_2O_5 compounds are quite stable at moderate temperatures; the degradation begins at about 200 °C. In this way, VG hybrid materials with sufficient thermal stability and low water contents can be interesting materials as positive electrodes for rechargeable lithium batteries.

Acknowledgements Financial support from CYCIT, Spain (projects MAT97-0326-CO4–01, MAT99-1217, and MAT2000-1585-C03-01), is gratefully acknowledged.

References

1. Livage J (1991) Chem Mater 3:578
2. Kamiyama T, Itoh T, Suzuki K (1988) J. Non-Cryst Solids 100:466
3. Ruiz-Hitzky E, Casal B (1986) J Chem Soc Faraday Trans I 82:1597
4. Casal B, Ruiz-Hitzky E, Crespin M, Tinet D, Galván JC (1989) J Chem Soc Faraday Trans I 85:4167
5. Bouhaouss A, Aldebert P, Baffier N, Livage J (1985) Rev Chim Miner 22:417
6. Van Damme H, Letellier M, Tinet D, Kihal B, Erre R (1984) Mater Res Bull 19:1635
7. Aldebert P, Paul-Boncour V (1983) Mater Res Bull 18:1263
8. Kanatzidis MG, Wu C-G, Marcy HO, Kannewurf CR (1989) J Am Chem Soc 111:4139
9. Leroux F, Koene BE, Nazar LF (1996) J Electrochem Soc 143:L181
10. Liu Y-J, DeGroot DC, Schindler JL, Kannewurf CR, Kanatzidis MG (1991) Chem Mater 3:992
11. Ruiz-Hitzky E, Aranda P, Casal B (1992) J Mater Chem 2:581
12. Kloster GM, Thomas JA, Brazis PW, Kannewurf CR, Shriver DF (1996) Chem Mater 8:2418
13. Goward G, Leroux F, Power WC, Nazar LF (1998) Electrochim Acta 43:1307
14. Leroux F, Goward G, Power WC, Nazar LF (1997) J Electrochem Soc 144:3886
15. Lira-Cantú MP, Gomez-Romero P (1999) J Electrochem Soc 146:2029
16. Sanchez C, Babonneau F, Morineu R, Livage J, Bullot J (1983) Philos Mag B 47:279
17. Babonneau F, Barboux P, Josien FA, Livage J (1985) J Chim Phys 82:761
18. Ramirez R, Casal B, Utrera L, Ruiz-Hitzky E (1990) J Phys Chem 27:8960
19. Yatanabe T, Matsubayashi G (1996) J Mater Chem 6:1849
20. Ackermans B, Schoonheydt RA, Ruiz-Hitzky E (1996) J Chem Soc Faraday Trans 92:4479
21. Casal B, Ruiz-Hitzky E (1988), Insertion et reactivité despeces organiques dans lespace intracristallin des xerogels V_2O_5. Communication to the 3rd Congrès National de la Société Française de Chimie, SCF 88, Nice, France. Abstracts, p 8P26
22. Ruiz-Hitzky E (1993) Adv Mater 5:334
23. Ruiz-Hitzky E, Aranda P (1997) An Quim Int Ed 93:197
24. Aranda P, Casal B, Galván JC, Ruiz-Hitzky E (1993) In: Bernier P, Fischer JE, Roth S, Solin SA (eds) Chemical physics of intercalation II. NATO ASI series B, vol 305. Plenum, New York, pp 397–400
25. Liu Y-J, Schindler JL, DeGroot DC, Kannewurf CR, Hirpo W, Kanatzidis MG (1996) Chem Mater 8:525
26. Barboux P, Baffier N, Morineau R, Livage J, (1983) Solid State Ionics 9/10:1073
27. Szörényi T, Bali K, Hevesi I (1985) J Phys 46:473
28. Badot JC, Fourrier-Lamer A, Baffier N (1985) J Phys 46:2107
29. Uchida N, Kittaka S (1994) J Phys Chem 98:2129
30. Bouhaouss A, Aldebert P (1983) Mater Res Bull 18:1247
31. Okuno S, Matsubayashi G (1993) Bull Chem Soc Jpn 66:459
32. Fabré J-M, Garín J, Uriel S (1991) Tetrahedron Lett 32:6407
33. Ruiz–Hitzky E, Casal B (1986) In: Setton R (ed) Chemical reactions in organic and inorganic constrained systems. NATO-ASI series C, vol 165. Reidel, Dordrecht, pp 179–189
34. Casal B, Ruiz-Hitzky E (1985) Opt Pura Apl 18:49
35. Vandenborre MT, Prost R, Huard E, Livage J (1983) Mater Res Bull 18:1133
36. White JL, Burns AF (1963) Science 141:800
37. Izatt RM, Bradshaw JS, Nielsen SA, Lamb JD, Christensen JJ (1985) Chem Rev 85:271
38. Buschmann HJ (1986) Inorg Chim Acta 118:77
39. Martinez-Lara M, Jimenez-Lopez A, Moreno-Real L, Bruque S, Casal B, Ruiz-Hitzky E (1985) Mater Res Bull 5:549

40. Masbah H, Tinet D, Crespin M, Erre R, Setton R, Van Damme H (1985) J Chem Soc Chem Commun 935
41. Erre R, Masbah H, Crespin M, Van Damme H, Tinet D (1990) Solid State Ionics 37:239
42. Van Damme H, Obrecht FG, Letellier M (1984) Nouv J Chim 8:681
43. Gilson TR, Bizri OF, Cheetham N (1973) J Chem Soc Dalton Trans 3:291
44. Sumathipala HH, Dissanayake MAKL, West AR (1995) J Electrochem Soc 142:21
45. Galván JC, Feliu S, Morcillo M (1989) Prog Org Coat 17:135
46. McCafferty E (1997) Corrosion Sci 39:243
47. Irvine S, Sinclair DC, West AR (1990) Adv. Mater. 2:132
48. Feliú S, Morcillo M, Galván JC (1989) J Electrochem Soc 1389:280
49. Feliú S, Galván JC, Morcillo M (1990), Corrosion Sci 30:989
50. Aranda P, Galván JC, Casal B, Ruiz–Hitzky E (1992) Electrochim Acta 37:1573